



**HAL**  
open science

## Generation of Gravity-Capillary Wind Waves by Instability of a Coupled Shear-Flow

Malek Abid, Christian Kharif, Hung-Chu Hsu, Yang-Yih Chen

► **To cite this version:**

Malek Abid, Christian Kharif, Hung-Chu Hsu, Yang-Yih Chen. Generation of Gravity-Capillary Wind Waves by Instability of a Coupled Shear-Flow. *Journal of Marine Science and Engineering*, 2022, 10 (1), pp.46. 10.3390/jmse10010046 . hal-03547954

**HAL Id: hal-03547954**

**<https://hal.science/hal-03547954v1>**

Submitted on 7 Mar 2023


**HAL** is a multi-disciplinary open access archive for the deposit and dissemination of scientific research documents, whether they are published or not. The documents may come from teaching and research institutions in France or abroad, or from public or private research centers.

L'archive ouverte pluridisciplinaire **HAL**, est destinée au dépôt et à la diffusion de documents scientifiques de niveau recherche, publiés ou non, émanant des établissements d'enseignement et de recherche français ou étrangers, des laboratoires publics ou privés.



Distributed under a Creative Commons Attribution 4.0 International License

# Generation of gravity-capillary wind waves by instability of a coupled shear-flow

Malek Abid <sup>1,\*</sup> , Christian Kharif <sup>1</sup>, Hung-Chu Hsu <sup>2</sup> and Yang-Yih Chen <sup>2</sup>

<sup>1</sup> Aix Marseille Université, CNRS, Centrale Marseille, IRPHE UMR 7342, F-13384, Marseille, France; malek.abid@univ-amu.fr

<sup>2</sup> Department of Marine Environment and Engineering, National Sun Yat-sen University, Kaohsiung, Taiwan; hchsu@mail.nsysu.edu.tw

\* Correspondence: malek.abid@univ-amu.fr

**Abstract:** The theory of surface wave generation, in viscous flows, is modified by replacing the linear-logarithmic shear velocity profile, in the air, with the model proposed by van Driest (1956) which links smoothly the linear and logarithmic layers through the buffer layer. This profile includes the effects of air flow turbulence using a damped mixing-length model. In the water, an exponential shear velocity profile is used. It is shown that this modified and coupled shear-velocity profile gives a better agreement with experimental data than the coupled linear-logarithmic, non smooth profile, (in the air)–exponential profile (in the water), widely used in the literature. We also give new insights on retrograde modes that are Doppler shifted by the surface velocity at the air-sea interface, namely on the threshold value of the surface current for the occurrence of a second unstable mode discovered by Zeisel *et al* (2008).

**Keywords:** Orr-Sommerfeld equation; wind waves; gravity; capillarity; shear flows; instability

## 1. Introduction

An important literature has been devoted to the generation of gravity-capillary waves at the sea surface under the action of a turbulent wind. The occurrence of gravity-capillary waves has been considered theoretically as the stability of a viscous parallel shear flow of air over water. Note that several studies have considered inviscid fluids, too. For a review on can refer to the paper by Young & Wolfe (2014). In the present paper we focus attention on viscous fluids and take into account the shear-induced flow (figure 1). Miles (1962) investigated the energy transfer from wind to short water waves through the viscous stress in the vicinity of the surface and neglected the shear flow in the water. He suggested that the generation of the short waves is due to a resonance mechanism between the water waves and the Tollmien-Schlichting waves occurring in the air shear flow. Within the framework of the Orr-Sommerfeld equation, Valenzuela (1976) investigated numerically the linear stability of the basic state composed of lin-log profiles in the water and in the air. He showed that the initial growth of the gravity-capillary wind waves is due to the linear instability of the parallel shear flow and that the water shear flow cannot be ignored. He found that the uncoupled model of Miles underestimates and overestimates the growth rate of waves of small and large wavenumbers, respectively. Kawai (1976) carried out experimentally and numerically the study of the same problem. He found that the frequency and the growth rate of the gravity-capillary waves depend on the air friction velocity and do not depend on the fetch. The basic coupled shear flow, composed of the lin-log profile in the air and an analytic functional form for the velocity profile in the water initially proposed by Kunishi (1957), was investigated numerically by using the Orr-Sommerfeld equation. He claimed that the amplification of infinitesimal disturbances inevitably present in the flow is due the instability of the basic state. Larson & Wright (1975) used

**Citation:** Abid, M.; Kharif, C.; Hsu, H.; Chen, Y.Y. Generation of gravity-capillary wind waves by instability of a coupled shear-flow. *J. Mar. Sci. Eng.* **2021**, *1*, 0. <https://doi.org/>

Received:  
Accepted:  
Published:

**Publisher's Note:** MDPI stays neutral with regard to jurisdictional claims in published maps and institutional affiliations.

**Copyright:** © 2021 by the authors. Submitted to *J. Mar. Sci. Eng.* for possible open access publication under the terms and conditions of the Creative Commons Attribution (CC BY) license (<https://creativecommons.org/licenses/by/4.0/>).

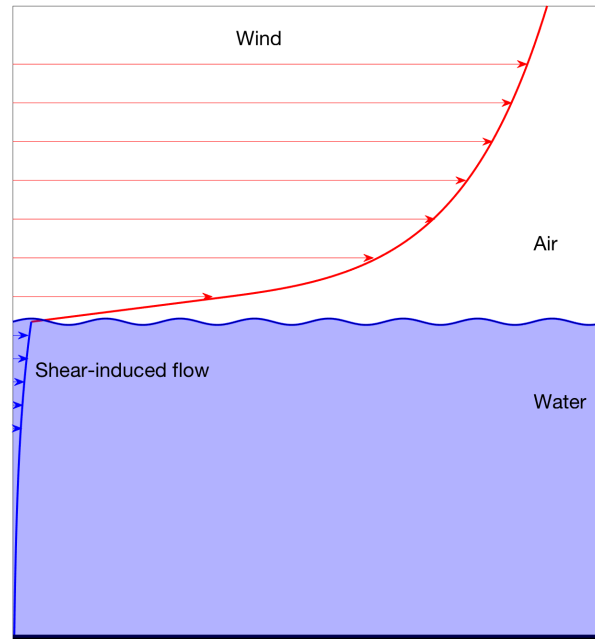


**Figure 1.** A Coupled shear flow. The wind blows up. Viscous effects induce a shear velocity profile in the water. Two boundary layers with high shear develop near the air-water interface. Consequently, the air-water interface is unstable and there is a growth of small water waves.

37 microwave backscatter based on the resonant Bragg scattering mechanism to measure  
 38 experimentally at fixed fetch the growth rates of wind induced gravity-capillary waves.  
 39 They found the growth rate does not depend on fetch. Furthermore, they proposed a  
 40 power law for the growth rate depending only the wavenumber of the water waves and  
 41 the friction velocity. van Gastel *et al.* (1985) tackled the problem of the linear stability of  
 42 the basic state using asymptotic methods to solve the Orr-Sommerfeld equation. They  
 43 considered the lin-log velocity profile in the air and an exponential velocity profile in  
 44 the water. They showed that the maximum growth rate is proportional to  $u_{*a}^3$  where  
 45  $u_{*a}$  is the air friction velocity. Note that Kawai (1976) found that the maximum growth  
 46 rate depends on  $u_{*a}^{3.5}$ . They concluded that the wave growth is mainly due to pressure  
 47 work resulting from normal pressure perturbation of the air on the surface. Wheless  
 48 & Csanady (1993) used a compound matrix method to integrate the Orr-Sommerfeld  
 49 equation. To avoid the unphysical discontinuity of the second derivative of the velocity  
 50 profile in the air existing in the previous models, they considered a velocity profile in  
 51 the air with a smooth variation of the second derivative and an exponential velocity  
 52 profile in the water. Note that the presence of discontinuities in the velocity profile in  
 53 the air may be troublesome computationally. They emphasized the influence of the  
 54 second derivative of the velocity profile in the air on the growth rate. As van Gastel *et al.*  
 55 (1985) they found that the growth rate of the gravity-capillary waves increases as  $u_{*a}^3$ .  
 56 Tsai & Lin (2004) extended numerically the stability of the coupled air-water shear flow  
 57 investigated analytically by van Gastel *et al.* (1985). They used a lin-log velocity profile in  
 58 the air and an exponential velocity profile in the water. Zeisel *et al.* (2008) investigated  
 59 numerically the temporal and spatial growth rates of short waves. They extended the  
 60 results of previous studies to larger wavelengths (up to 20 cm) and stronger winds (up  
 61 to  $u_{*a} \sim 1 \text{ m.s}^{-1}$ ). Their main finding is the occurrence of a second unstable mode when  
 62  $u_{*a} > 0.5 \text{ m.s}^{-1}$ . Our main purpose focuses on the occurrence condition of the second  
 63 unstable mode discovered by Zeisel *et al.* (2008). In the present study, the theory of surface  
 64 wave generation, in viscous flows, is modified by replacing the linear-logarithmic shear  
 65 velocity profile, in the air, with the model proposed by van Driest (1956) which links  
 66 smoothly the linear and logarithmic layers through the buffer layer. This profile includes  
 67 the effects of air flow turbulence using a damped mixing-length model. In the water, an

68 exponential shear velocity profile is used. Note that Riley *et al.* (1982) used the model  
 69 proposed by van Driest to study wave generation by wind, but in the context of Miles'  
 70 theory, i.e. with inviscid flows and no current in the water. The paper is organized as  
 71 follows. The mathematical model is presented in section 2. Section 3 is devoted to the  
 72 presentation of the velocity profiles in the air and in the water. A particular attention is  
 73 paid to the velocity profile introduced by van Driest (1956). The developed numerical  
 74 method and its validation are presented in section 4. Finally, we present our main results  
 75 in section 5 and our conclusions are given in section 6.

## 76 2. Mathematical model

77 We consider the stability of a basic state  $(U_0(z), P_0(z))$  to small perturbations  
 78  $\mathbf{u}(x, z, t) = (u, w)$  and  $p(x, z, t)$  where  $U_0(z)$  is the mean velocity profile,  $P_0(z)$  the  
 79 static pressure,  $t$  the time,  $x$  and  $z$  the horizontal and vertical coordinates, respectively.  
 80 The continuity equation and the linearized Navier-Stokes equation read

$$\frac{\partial u}{\partial x} + \frac{\partial w}{\partial z} = 0 \quad (1)$$

$$\frac{\partial u}{\partial t} + U_0 \frac{\partial u}{\partial x} + w \frac{\partial U_0}{\partial z} = -\frac{1}{\rho} \frac{\partial p}{\partial x} + \nu \left( \frac{\partial^2 u}{\partial x^2} + \frac{\partial^2 u}{\partial z^2} \right) \quad (2)$$

$$\frac{\partial w}{\partial t} + U_0 \frac{\partial w}{\partial x} = -\frac{1}{\rho} \frac{\partial p}{\partial z} + \nu \left( \frac{\partial^2 w}{\partial x^2} + \frac{\partial^2 w}{\partial z^2} \right) \quad (3)$$

where  $\rho$  and  $\nu$  are the density and kinematic viscosity, respectively.  
 The solutions of the linearized problem are sought in the form

$$(u, w, p) = (u_1(z), w_1(z), p_1(z)) \exp[ik(x - ct)]$$

81 where  $k$  is the wavenumber of the perturbation and  $c$  its complex velocity. Note that the  
 82 growth rate of the perturbation is  $\omega_i = \Im(kc)$  and the energy growth rate is  $\beta = 2\omega_i$ .  
 83 The system of equations (1)-(3) gives

$$iku_1 + \frac{dw_1}{dz} = 0 \quad (4)$$

$$ikWu_1 + w_1 \frac{dW}{dz} = -\frac{ikp_1}{\rho} + \nu \left( \frac{d^2 u_1}{dz^2} - k^2 u_1 \right) \quad (5)$$

$$ikWw_1 = -\frac{1}{\rho} \frac{dp_1}{dz} + \nu \left( \frac{d^2 w_1}{dz^2} - k^2 w_1 \right) \quad (6)$$

where  $W = U_0(z) - c$ .

After simple algebraic calculations the system of equations (4)-(6) reduces to the following differential equation (Orr-Sommerfeld equation)

$$iW \left( \frac{d^2}{dz^2} - k^2 \right) w_1 - i \frac{d^2 W}{dz^2} w_1 = \frac{\nu}{k} \frac{d^4 w_1}{dz^4} - 2\nu k \frac{d^2 w_1}{dz^2} + \nu k^3 w_1 \quad (7)$$

84 Note that the left-hand side of equation (7) corresponds to the Rayleigh equation.

85 The system of differential equations to solve is

$$\frac{\nu_a}{k} \left( \frac{d^2}{dz^2} - k^2 \right)^2 w_1 = iW \left( \frac{d^2}{dz^2} - k^2 \right) w_1 - i \frac{d^2 W}{dz^2} w_1 \quad (8)$$

$$\frac{\nu_w}{k} \left( \frac{d^2}{dz^2} - k^2 \right)^2 w_1 = iW \left( \frac{d^2}{dz^2} - k^2 \right) w_1 - i \frac{d^2 W}{dz^2} w_1 \quad (9)$$

where the subscripts  $a$  and  $w$  refer to the air and water, respectively. At first-order, the amplitude  $p_1$  of the wave pressure can be derived from the horizontal component of the linearized Navier-Stokes equation

$$p_1 = \frac{\rho}{ik} \left( W \frac{dw_1}{dz} - w_1 \frac{dW}{dz} \right) + \frac{\mu}{k^2} \left( \frac{d^3 w_1}{dz^3} - k^2 \frac{dw_1}{dz} \right) \quad (10)$$

where  $\mu = \rho\nu$  is the dynamic viscosity.

Using a Taylor expansion about  $z = 0$ , the first-order continuity condition for the normal stress at the interface  $\eta(x, t) = \eta_1 \exp[ik(x - ct)]$  reads

$$p(x, 0+, t) - p(x, 0-, t) = 2\mu_a \frac{\partial w}{\partial z}(x, 0+, t) - 2\mu_w \frac{\partial w}{\partial z}(x, 0-, t) + T \frac{\partial^2 \eta}{\partial x^2} + (\rho_a - \rho_w)g\eta \quad (11)$$

where  $T$  is the surface tension,  $g$  the acceleration due to gravity,  $\mu_a = \rho_a \nu_a$  and  $\mu_w = \rho_w \nu_w$ .

The linearized kinematic boundary condition about  $z = 0$  is

$$\left( \frac{\partial}{\partial t} + U_s \frac{\partial}{\partial x} \right) \eta = w$$

where  $U_s = U_0(0)$ .

From this equation one can derive

$$\eta_1 = \frac{w_1(0)}{ikW(0)} \quad (12)$$

with  $W(0) = U_s - c$ .

Combining equations (10), (11) and (12) gives *in fine* the first-order continuity condition for the normal stress at the interface

$$\begin{aligned} \rho_a \left\{ W(0) \left( W(0)w_1'(0+) - W'(0+)w_1(0) \right) + i\nu_a \frac{W(0)}{k} \left( w_1'''(0+) - 3k^2 w_1'(0+) \right) - gw_1(0) \right\} = \\ \rho_w \left\{ W(0) \left( W(0)w_1'(0-) - W'(0-)w_1(0) \right) + i\nu_w \frac{W(0)}{k} \left( w_1'''(0-) - 3k^2 w_1'(0-) \right) - Gw_1(0) \right\}. \end{aligned} \quad (13)$$

The prime denotes  $d/dz$  and  $G = g + Tk^2$ . Note that we can use  $w_1(0) = ikW(0)\eta_1$ .

Using a Taylor expansion about  $z = 0$ , the first-order continuity condition for the tangential stress at the interface reads

$$\mu_a \left\{ \frac{\partial w}{\partial x}(x, 0+, t) + \frac{\partial}{\partial z}(u + \eta W')(x, 0+, t) \right\} = \mu_w \left\{ \frac{\partial w}{\partial x}(x, 0-, t) + \frac{\partial}{\partial z}(u + \eta W')(x, 0-, t) \right\} \quad (14)$$

Using  $u_1' = -w_1''/(ik)$  the boundary condition at the interface for the tangential stress becomes

$$\begin{aligned} \mu_a \left\{ w_1(0)W''(0+) - W(0) \left( w_1''(0+) + k^2 w_1(0) \right) \right\} = \\ \mu_w \left\{ w_1(0)W''(0-) - W(0) \left( w_1''(0-) + k^2 w_1(0) \right) \right\} \end{aligned} \quad (15)$$

86 The continuity of the vertical and horizontal components of fluid velocity at the interface

87 reads

$$\begin{aligned} w(x, 0+, t) &= w(x, 0-, t) \\ u(x, 0+, t) + \eta W'(0+) &= u(x, 0-, t) + \eta W'(0-) \end{aligned}$$

88 Using  $u_1 = -w_1'/(ik)$  the fluid velocity continuity at the interface becomes

$$w_1(0+) = w_1(0-) = w_1(0) \quad (16)$$

$$w_1'(0+)W(0) - w_1(0)W'(0+) = w_1'(0-)W(0) - w_1(0)W'(0-) \quad (17)$$

Far from the interface all perturbations should vanish. Therefore

$$\lim_{z \rightarrow \pm\infty} w_1(z) = 0. \quad (18)$$

### 89 3. Velocity profiles

90 The theoretical study of the generation of water waves by wind relies on the  
91 hypothesis that the mean velocities in the turbulent boundary layers (in the air and in  
92 the water) may be regarded as parallel shear flows (figure 1). It is also well known that  
93 the results of instability studies are sensitive to the velocity profile shape. In this section,  
94 details concerning the mean flows used, herein, in the air and in the water are given.

#### 95 3.1. Air profiles

96 The exact mean turbulent profile above water waves is not well known. As infinitesimal waves are studied, it is a good approximation to consider mean flow profiles above  
97 flat plates. Two profiles have retained our attention, the lin-log profile and the damped  
98 mixing-length profile.  
99

##### 100 3.1.1. The lin-log profile

The widely used velocity profile, for water wave generation by wind, is called the lin-log profile. It is linear in a viscous sublayer and is asymptotically logarithmic far from the interface. The lin-log velocity profile, used in previous studies, reads (Zeisel *et al.* (2008)):

$$U_a = \begin{cases} U_s + \frac{u_*^2}{\nu_a} z, & 0 \leq z \leq z_1, \\ U_s + m u_* + \frac{u_*}{\kappa} \left[ \alpha - \tanh\left(\frac{\alpha}{2}\right) \right], & z \geq z_1 \end{cases} \quad (19)$$

$$\alpha = \sinh^{-1}(\beta), \quad \beta = \frac{2\kappa u_*}{\nu_a} (z - z_1), \quad z_1 = \frac{m\nu_a}{u_*}, \quad U_s = B u_*, \quad m = 5, \quad B = 0.5. \quad (20)$$

##### 101 3.1.2. The mixing-length profile

For a boundary layer in the air, according to the Prandtl mixing length hypothesis, the total shear stress near the air-sea interface is

$$\frac{\tau_a(z)}{\rho_a} = \nu_a \frac{\partial U_a}{\partial z} + \nu_T \frac{\partial U_a}{\partial z}, \quad (21)$$

where  $\nu_T$  is the turbulent viscosity given by  $\nu_T = \ell_m \partial U_a / \partial z$  and  $\ell_m(z)$  is the mixing length. Using the following normalisations:

$$U_a^+ = U_a / u_*, \quad z^+ = u_* z / \nu_a, \quad \tau^+ = \tau_a / (\rho_a u_*^2), \quad \ell_m^+ = u_* \ell_m / \nu_a, \quad (22)$$

the total shear stress reads

$$\frac{\tau_a(z)}{\tau_a^+} = \frac{\partial U_a^+}{\partial z^+} + (\ell_m^+ \frac{\partial U_a^+}{\partial z^+})^2. \quad (23)$$

The solution of this quadratic equation for  $\partial U_a^+ / \partial z^+$  is

$$\frac{\partial U_a^+}{\partial z^+} = \frac{2\tau_a / \tau_a^+}{1 + [1 + (4\tau_a / \tau_a^+) (\ell_m^+)^2]^{(1/2)}}. \quad (24)$$

102 Near the air-sea interface, the ratio  $\tau_a(z)/\tau_a^+$  is practically unity so that

$$U_a^+(z^+) = \int_0^{z^+} \frac{2}{1 + \sqrt{1 + 4\ell_m^+(z')^2}} dz'. \quad (25)$$

103 For large  $z^+$ , where viscosity effect is small, the mixing length is  $\ell_m^+ = \kappa z^+$  and the log  
 104 law is recovered when constant terms in the integrand denominator are neglected in the  
 105 limit  $z^+ \rightarrow +\infty$ . If the same specification for the mixing length is used near the air-sea  
 106 interface (in the viscous sublayer) considered as rigid (a wall), the resulting turbulent  
 107 stress  $\nu_T \partial U_a / \partial z$  will increase as  $z^2$ , whereas the Reynolds stress  $-\langle uw \rangle$  increases more  
 108 slowly, as  $z^3$  (Pope (2000)). Therefore, the specification  $\ell_m = \kappa z$  needs to be damped near  
 109 the interface and van Driest (1956) proposed

$$\ell_m^+(z^+) = \kappa [1 - \exp(-z^+ / A^+)], \quad (26)$$

110 where  $A^+$  is a constant attributed the value  $A^+ = 26$ .

111 The van Driest and the lin-log velocity profiles are compared in figure 2 together  
 112 with experimental data from Eckelmann (1974) and direct numerical-simulation results  
 113 from Kim *et al.* (1987). The law of the wall is also shown. Normalised coordinate  $z^+$   
 114 and velocity  $U_a^+$  are used. The different profiles are practically undistinguishable for  
 115  $z^+ \leq 10$ . However, It is clear that the van Driest profile fits better with experimental  
 116 data and numerical simulations than the lin-log profile for  $z^+ > 10$ . Furthermore, the  
 117 main advantage of the van Driest profile is the fact that it is infinitely derivable, i.e.  
 118  $C^\infty$ , contrarily to the lin-log profile who is piecewise defined and hence not infinitely  
 119 derivable. This is shown in figure 3.

### 120 3.2. Water profile

Many velocity profiles have been used in the water, in previous studies, and are  
 reported in figure 1 of van Gastel *et al.* (1985). Among them the exponential profile has  
 retained our attention because it resembles experimental observations (Kawai 1979) and  
 because it allows for exact solution of the Rayleigh equation that will be used below  
 to compute sheared gravity-capillary wave speeds. In the water, the current profile is  
 (Zeisel *et al.* (2008))

$$U_w(z) = U_s \exp\left(\frac{\rho_a u_*^2}{U_s \mu_w} z\right), \quad z < 0. \quad (27)$$

## 121 4. Numerical method and validation

122 The differential equation (7) and boundary conditions (13), (15), (16), (17) and (18)  
 123 are transformed into an algebraic system of equations using a spectral Tau approximation  
 124 method (Gottlieb and Orszag (1977)). This algebraic system of equations is solved  
 125 numerically for  $w_1$  and  $c$  for a given wavenumber  $k$ . Note that the algebraic system is  
 126 nonlinear in  $c$  due to the boundary condition (13). Therefore, the Levenberg-Marquardt  
 127 method (Moré (1977)) is used and computations are stopped when the residual is  
 128  $O(10^{-12})$ . We also used the Broyden method (Broyden (1965)). The boundary conditions  
 129 at infinity are enforced at  $z_{\pm\infty} = \pm 1.6 \lambda$  where  $\lambda = 2\pi/k$  is the reference wavelength  
 130 (Zeisel & al. (2008)). This choice corresponds to  $kz_{\pm\infty} \simeq \pm 10$ . We have checked  
 131 that doubling  $z_{\pm\infty}$  does not affect significantly the results. The obtained results are  
 132 validated by (a) the self consistency of the results from Levenberg-Marquardt and  
 133 Broyden methods and (b) by comparisons with already published results in the literature  
 134 obtained with the lin-log velocity profile in the air. The sum up of these comparisons is  
 135 given in figure 4.

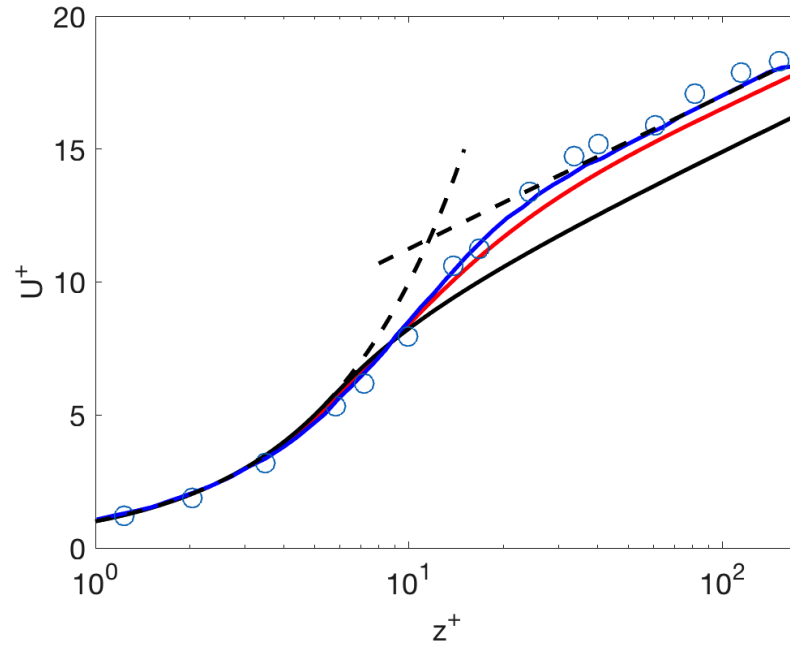


**Figure 2.** Colour on-line. Normalised velocity profiles, in the air, against the normalised  $z$  coordinate. Blue: direct numerical simulations of Kim *et al.* (1987).  $\circ$  Eckelmann (1974) experimental data. Red: van Driest (1956) profile. Black: lin-log profile. Discontinuous line: law of the wall.

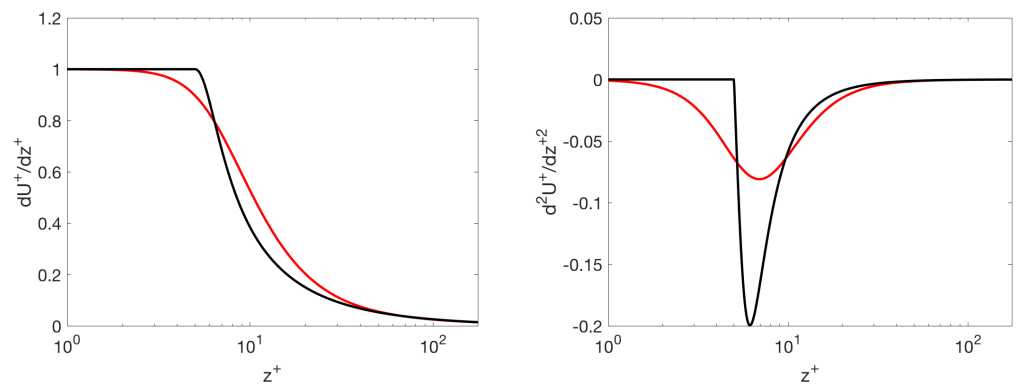


**Figure 3.** Colour on-line. Normalised derivatives of the van Driest velocity profile (in red) and the lin-log profile (in black), against the normalised  $z$  coordinate. Left: first derivative and right: the second derivative. Note the sharp discontinuity of the second derivative for the lin-log profile.



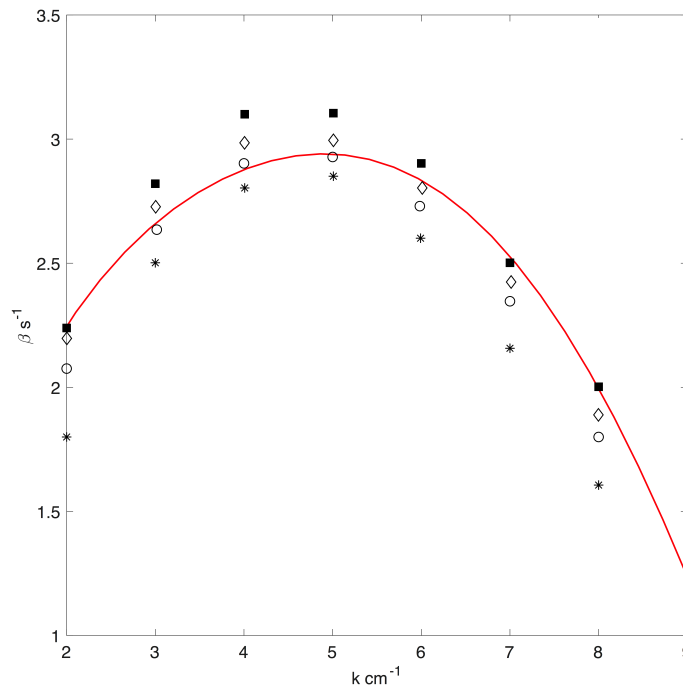


**Figure 4.** Color on line. Validation of the numerical method, for  $u_* = 24.8 \text{ cm s}^{-1}$ , using the lin-log velocity profile in the air and the exponential profile in the water. The energy growth rate  $\beta$  is plotted against the wavenumber  $k$ . Present results: solid line (red). Zeisel *et al.* (2008):  $\diamond$ . Kawai (1979):  $\blacksquare$ . van Gastel *et al.* (1985):  $\blacksquare$ . Tsai & Lin (2004):  $*$ .  $\circ$ .

## 136 5. Results

### 137 5.1. Prograde unstable modes

138 Using the above described Orr-Sommerfeld equations, and the appropriate bound-  
 139 ary conditions, we have computed the maximum energy growth rate,  $\beta$ , for wavenum-  
 140 bers in the range  $1 < k < 9 \text{ (cm}^{-1}\text{)}$ , and for different values of the friction velocity  $u_*$ .  
 141 In this paragraph waves travelling with the wind (waves with positive intrinsic phase  
 142 speeds) are considered. The results are presented in figure 5 for the lin-log profile and  
 143 the van Driest profile in the air and exponential profile in the water. The results from  
 144 Kawai (1979) are also reported. The agreement using the van Driest profile is better  
 145 than that obtained with the lin-log profile. This fact could be justified by inspection  
 146 of the comparison of the different velocity profiles presented in figure 2. Indeed, the  
 147 lin-log profile departs from the other profiles far from the air-water interface. Besides,  
 148 the van Driest profile is infinitely derivable and this fact is an advantage for numerical  
 149 computations.

### 150 5.2. Retrograde unstable modes (Second mode)

Young & Wolfe (2014) have pointed out the existence of a second unstable mode, called rippling mode, in the context of inviscid fluids (using the Rayleigh equations). The maximum growth rate they obtained is  $O(1 \text{ s}^{-1})$  for  $k = O(4 \text{ cm}^{-1})$ . Noting that for these values  $v_a k^2 = O(2.4 \text{ s}^{-1})$ , the second mode will be obviously damped by viscosity in the context of Orr-Sommerfeld equations. Zeisel *et al.* (2008) have also discovered a second mode in the context of viscous flows when the air friction velocity is larger than  $50 \text{ cm s}^{-1}$ . In both cases, the second modes are retrograde modes (waves with negative intrinsic phase velocity) that are Doppler shifted by the surface velocity  $U_s$  in the wind direction (positive phase velocity). Therefore, a necessary condition for their occurrence is

$$c_0 \geq 0 \text{ and } c_0 - U_s \leq 0, \quad (28)$$

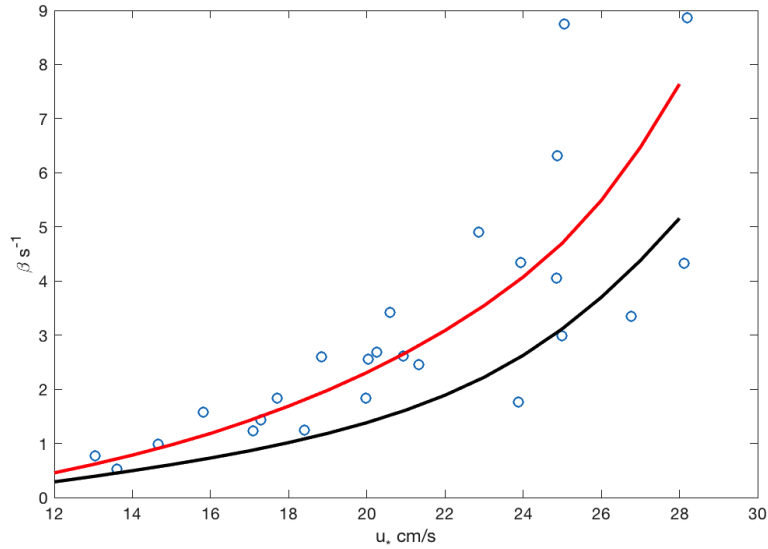


**Figure 5.** Colour on line. Comparison with experimental data. The energy growth rate  $\beta$  is plotted against the friction velocity  $u_*$ .  $\circ$  Kawai (1979) experimental results realized with  $u_* z_1 / \nu_a = 5$ , with  $z_1$  the height of the viscous layer in the air. Red: Theoretical values obtained using the van Driest velocity-profile in the air and the exponential profile in the water. Black: Theoretical values obtained using the lin-log velocity profile in the air and the exponential profile in the water.

where  $c_0$  should be the *sheared* gravity-capillary wave speed in the laboratory frame. Zeisel *et al.* have found a minimum value  $u_* \simeq 50 \text{ cm s}^{-1}$  corresponding to  $\lambda \simeq 3 \text{ cm}$  for the occurrence of the second mode. However, they used the gravity-capillary wave speed

$$c_0 = U_s \pm \sqrt{\frac{g}{k} + \gamma k}, \quad \gamma = \frac{T}{\rho_a}, \quad (29)$$

and not the sheared gravity-capillary one, as it should be, to justify these values (in their figure 13). Retrograde waves correspond to the minus sign before the square root. In the present study, we use the *sheared* gravity-capillary wave speed given by equation (6.3) of Young & Wolfe (2014) to predict the critical values. Note that this equation presents a typo that we have corrected. The corrected equation reads (with  $U_s > 0$  as it is the wind-induced surface drift),

$$c_0 = U_s \left[ 1 - \frac{1}{2\sqrt{1 + (h_w k)^2}} \pm \sqrt{\frac{(gh_w)/U_s^2 + (\gamma/(h_w U_s)^2)(h_w k)^2}{\sqrt{1 + (h_w k)^2}} + \frac{1}{4(1 + (h_w k)^2)}} \right], \quad (30)$$

and it is valid for gravity-capillary waves propagating on an exponential velocity profile in the water of the form  $\exp(z/h_w)$ , where  $h_w$  is the characteristic shear length. In the present study the characteristic shear length depends on air density, friction velocity (or equivalently on the surface velocity  $U_s$ ) and water viscosity. By inspection of equation (27) we have

$$h_w(U_s) = \frac{\mu_w}{4\rho_a U_s}.$$

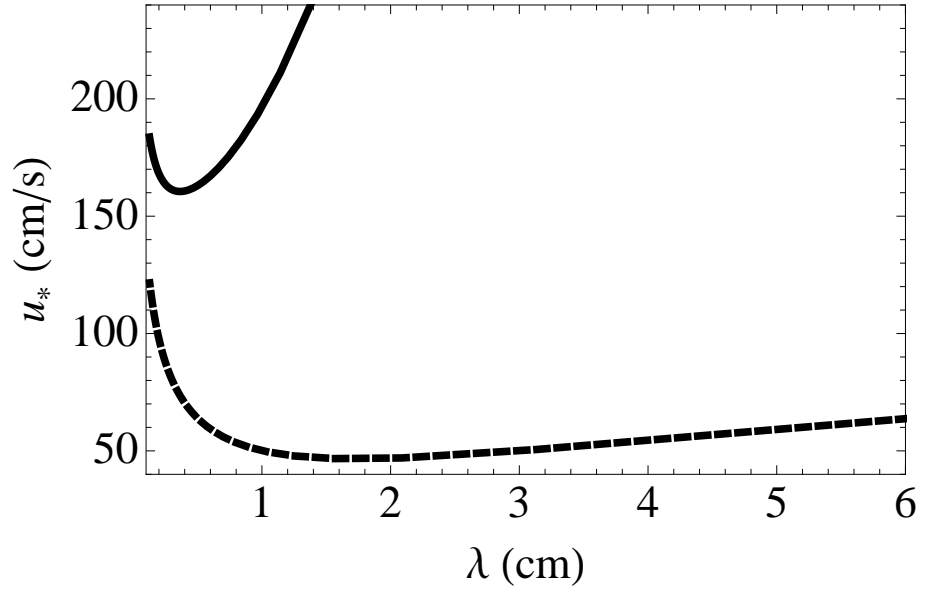


**Figure 6.** Critical value of  $u_*$  corresponding to the occurrence of the second mode is plotted against the wavelength  $\lambda$ . Continuous line: using the sheared gravity-capillary wave speed. The minimum value of  $u_*$ , for the occurrence of the second mode, is approximately  $u_* \simeq 160 \text{ cm s}^{-1}$  corresponding to a wavelength  $\lambda \simeq 0.35 \text{ cm}$ . Dashed line: using the gravity-capillary wave speed in still water. The minimum value of  $u_*$ , for the occurrence of the second mode, is approximately  $u_* \simeq 45 \text{ cm s}^{-1}$  corresponding to a wavelength  $\lambda \simeq 1.74 \text{ cm}$ .

Therefore, we obtain the following *implicit* equation for  $U_s$  to satisfy the necessary condition of the occurrence of the second mode:

$$U_s = \sqrt{\left(\frac{g}{k} + \gamma k\right) \left( \frac{4(\rho_a/\rho_w)U_s}{\nu_w k} + \sqrt{\left(1 + \left(\frac{4(\rho_a/\rho_w)U_s}{\nu_w k}\right)^2\right)} \right)}, \quad (31)$$

and the corresponding friction velocity is

$$u_* = 2U_s,$$

151 with in cgs units:  $g = 981$ ;  $\gamma = 75$ ;  $\mu_w = 10^{-2}$ ;  $\rho_a = 1.23 \cdot 10^{-3}$ . The Newton  
 152 method is used to solve the implicit equation (31) and the results are given in figure 6  
 153 using  $\lambda = 2\pi/k$  where  $\lambda$  is the wavelength. By inspection of this figure, the minimum  
 154 friction velocity for the occurrence of the second mode is  $u_* \simeq 160 \text{ cm s}^{-1}$  corresponding  
 155 to  $\lambda \simeq 0.35 \text{ cm}$ . Indeed, using the van Driest velocity profile in the air and the exponential  
 156 profile in the water, we have found no second mode for as high values of  $u_*$  as  $124 \text{ cm s}^{-1}$   
 157 (the highest value studied experimentally by Larson & Wright (1975)). Wheless &  
 158 Csanady (1993) have emphasized the sensitivity of the growth rate to the curvature of  
 159 the air velocity profile. Note that this fact does not call into question the existence of the  
 160 second mode.

## 161 6. Conclusions

162 We studied surface wave generation by wind in viscous flows. We focused on  
 163 gravity-capillary waves. Our main purpose was to use air velocity profile that avoids  
 164 the inherent discontinuity of the second derivative of the lin-log profile. That is why we  
 165 have considered the van Driest profile which links smoothly through the buffer layer  
 166 the linear and logarithmic layers. Our numerical computations of the rate of growth of  
 167 the gravity-capillary waves, with the van Driest profile, are in better agreement with the  
 168 experimental data of Kawai (1976) than those calculated with the lin-log profile.

169 Besides the unstable mode which occurs whatever the investigated values of the air  
 170 friction velocity, Zeisel & *et al.* (2008) discovered a new additional unstable mode for  
 171 strong winds when the air friction velocity is larger than approximately  $50 \text{ cm s}^{-1}$ . We  
 172 have developed eigenvalue computations until  $124 \text{ cm s}^{-1}$  (the highest value studied  
 173 experimentally by Larson & Wright (1975)) and did not find second mode instability  
 174 using the van Driest profile. A theoretical approach, based on the linear dispersion  
 175 relation of gravity-capillary waves travelling on an exponential current, showed that  
 176 the threshold value is close to  $160 \text{ cm s}^{-1}$  whereas it is close to  $50 \text{ cm s}^{-1}$  for a constant  
 177 current. This gap is probably due to the sensitivity of the growth rate to the profiles used  
 178 as mentioned by previous authors.

179 **Author Contributions:** Conceptualization, C.K. and Y.Y.C.; Methodology, C.K. and Y.Y.C.; Formal  
 180 Analysis, C.K., M.A. and H.C.H.; Writing M.A. and C.K.; Software, M.A.; Validation, M.A.;  
 181 Investigation, M.A., C.K. and H.C.H.; Visualization, M.A. All authors have read and agreed to the  
 182 published version of the manuscript.

183 **Funding:** This research was funded by the Excellence Initiative of Aix-Marseille University—A\*Midex,  
 184 a French “Investissements d’Avenir programme” AMX-19-IET-010.

185 **Data Availability Statement:** Data available on demand.

186 **Conflicts of Interest:** “The authors declare no conflict of interest.”

## References

1. Broyden, C. G., A Class of Methods for Solving Nonlinear Simultaneous Equations. *Mathematics of Computation, American Mathematical Society* **1974**, *19* (92), 577–593.
2. Eckelmann H., The structure of the viscous sublayer and the adjacent wall region in a turbulent channel flow. *J. Fluid Mech* **1974**, *65*, 439–459.
3. Gottlieb D. and Orszag S. A. *Numerical Analysis of Spectral Methods: Theory and Applications*; Siam: Philadelphia, Pennsylvania, U. S. A., **1977**, 11–13.
4. Kawai S., Generation of initial wavelets by instability of a coupled shear flow and their evolution to wind waves. *J. Fluid Mech* **1979**, *93*, 661–703.
5. Kim J., Moin P. and Moser R., Turbulence statistics in fully developed channel flow at low Reynolds number. *J. Fluid Mech* **1987**, *177*, 133–166.
6. Kunishi H., Studies on wind waves with use of wind flume. (I) On the shearing flow in the surface boundary layer caused by wind stress. *Ann. Disas. Prev. Res. Inst., Kyoto Univ.* *1*, 119–127.
7. Larson T. R. and Wright J. W., Wind-generated gravity-capillary waves: laboratory measurements of temporal growth rates using microwave backscatter. *J. Fluid Mech* **1975**, *70*, 417–436.
8. Miles J. W., On the generation of surface waves by shear flows. Part 4. *J. Fluid Mech* **1962**, *13*, 433–448.
9. Moré, J. J., The Levenberg-Marquardt Algorithm: Implementation and Theory, *Numerical Analysis*, ed. G. A. Watson, Lecture Notes in Mathematics, 630, Springer Verlag, **1977**, 105–116.
10. Riley D. S., Donelan M. A., and Hui W. H., An extended Miles’ theory for wave generation by wind. *Boundary Layer Methodology* **1982**, *22*, 209–225.
11. Tsai W-T and Lin M-Y, stability analysis on the initial surface-wave generation with an air-sea coupled shear flow. *J. Marine Sci. Tech.* **2004**, *597*, 200–208.
12. Valenzuela G. R., The growth of gravity-capillary waves in a coupled shear flow. *J. Fluid Mech* **1976**, *76*, 229–250.
13. van Driest E. R., On turbulent flow near a wall. *J. Aerospace Sci* **1956**, *23*, 1007–1011.
14. van Gastel K., Janssen P. A. E. M. and Komen G. J., On phase velocity and growth rate of wind-induced gravity-capillary waves. *J. Fluid Mech* **1985**, *161*, 199–216.
15. Wheless G. W. and Csanady G. T., Instability waves on the air-sea interface. *J. Fluid Mech* **1993**, *248*, 363–381.
16. Young W. R. and Wolfe C. L., Generation of surface waves by shear-flow instability. *J. Fluid Mech* **2014**, *739*, 276–307.
17. Zeisel A., Stiassnie M. and Agnon Y., Viscous effects on wave generation by strong winds. *J. Fluid Mech* **2008**, *597*, 343–369.